Towards Building Smart Self-Folding Structures

Edwin Alexander Peraza Hernandez[a], Shiyu Hu[a], Han Wei Kung[a], Darren Hartl[a], Ergun Akleman[a]

[a]*Texas A&M University*

Abstract

We report our initial progress on synthesizing complex structures from programmable self-folding active materials, which we call Smart Multi-Use Reconfigurable Forms. We have developed a method to unfold a given convex polygonal mesh into a one-piece planar surface. We analyze the behavior of this surface as if it were constructed from realistic active materials such as shape memory alloys (SMAs), in which sharp creases and folds are not feasible. These active materials can change their shapes when they are heated and have been applied to medical, aerospace, and automotive applications in the engineering realm. We demonstrate via material constitutive modeling and utilization of finite element analysis (FEA) that by appropriately heating the unfolded planar surface it is possible to recover the 3D shape of the original polygonal mesh. We have simulated the process and our finite element analysis simulations demonstrate that these active materials can be raised against gravity, formed, and reconfigured automatically in three dimensions with appropriate heating in a manner that extends previous work in the area of programmable matter. Based on our results, we believe that it is possible to use active materials to develop reprogrammable self-folding complex structures.

Keywords: Shape Modeling, Physical Construction, Finite Element Analysis, Active Materials, Shape Memory Alloys, Physically Based Modeling, Programmable Matter

1. Motivation

This paper presents our initial progress for realization of complex and reconfigurable 3D surfaces and structures that are assembled from "programmable" 2D planar shapes made of self-folding active materials. Our goal is to develop structures that can be raised, formed, and reconfigured automatically in 3-space as depicted in the artistic interpretation in Figure 1. In this paper we present a framework for modeling the geometry of the active material elements that can self-fold into a desired 3D shape and we demonstrate that these elements can be folded to create desired shapes. In our framework, we start with a polygonal mesh approximation of the desired 3D shape. Then, we unfold it into either multiple or single-piece planar panels, which are simply 2D polygons. By physically and virtually construct the original shapes, we demonstrate the feasibility of this approach, which is well-suited for the consideration of deforming materials in which sharp folds or creases are not physically feasible. Our results can be summarized as follows:

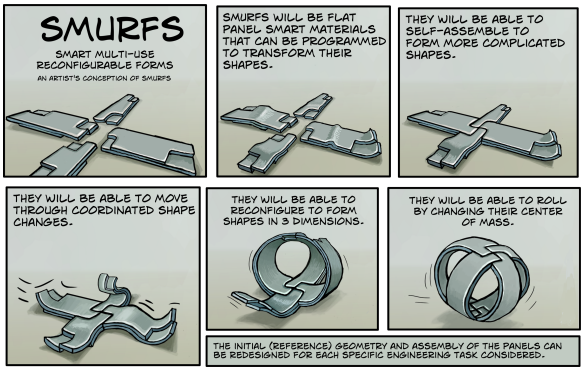

Figure 1: An artistic representation of the ultimate goals of research on self-folding structures as smart multi-use reconfigurable forms.

Multi-Panel Unfolding and Physical Construction: (1) We have developed an approach to unfold any given polygonal mesh surface into a set of planar pieces. (2) We have developed and implemented a method to construct physical shapes that approximate original polygonal meshes by connecting and folding the planar pieces. (3) We have constructed a few examples of physical shapes using planar pieces to demonstrate the feasibility of the approach.

Single-Panel Unfolding and Evaluation of Construction: (1) We have extended the multi-panel unfolding method to reduce the number of planar pieces into one to be cut from a single sheet of continuous self-folding active materials. To unfold into a non-self-intersecting single-panel (i.e. a simple 2D polygon), the main restriction is that the original shape must be convex. If the shape is not convex, it can still be unfolded into a 2D polygon, but the resulting polygon can self-intersect. For single panel unfolding (2) we have created a few examples of unfolded single-panels and have physically constructed shapes using single-panels that are cut from paper and (3) we have evaluated self-folding behavior single panels that are cut from self-folding active materials using Abaqus, a physics-based Finite Element Analysis program. Favorable results indicate that we can obtain the same behavior once self-folding active materials are available. A useful property of this approach is that unfolding is not unique, i.e., there exists many 2D polygons that can be folded into a given desired shape. Because of this property, it is possible to allow engineers or artists to choose from a finite set the 2D shape of unfolded polygon.

2. Previous Work

The efforts described in this work were inspired by the bodies of existing literature associated with two topical areas: paper sculpture/origami and morphing structures. The methods and advantages of paper-based design and analysis have been receiving an increasing amount of attention in the past few years [1, 2], and the mathematical framework associated with these methods has continued to develop [3, 4, 5]. Moreover, methods to obtain paper sculptures and origami from any given polyhedral meshes are developed [6, 7]. Though motivated in part by this progress, here we relax some of the restrictions of conventional origami theory (infinitely sharp folds, perfectly flat panels) and instead consider shape changes that could be obtained using active materials to drive the required deformations [8, 9]. The combination of smart materials and origami research has previously given rise to the concept of *programmable matter* [10], though again, sharp folds and flat panels were an explicit goal. Other researches exist that also consider predefined folds in active materials [11, 12].

In this work, a self-folding laminate including two shape memory alloy (SMA) thin film layers [13, 14] that provide force and high deformation under the imposition of heat is considered. These active lamina are separated by a relatively compliant passive (e.g., elastomeric) layer. This approach is novel in that it eliminates the need for local predefined hinges as fold locations are simply determined by where heat is applied to the SMA. The location and intensity of heating can be changed over time, resulting in "massively reconfigurable" self-folding structures, where local fold angles may be relatively large (i.e., folds may not be sharp). This concept was only recently introduced [15], and it was shown via methods similar to those considered herein that such a laminate sheet could be configured to provide multiple shapes. Studies have continued [16], demonstrating that replacing the SMA thin film by a mesh of SMA wire might provide significant advantages.

After a description of the approaches used to "unfold" a desired three-dimensional form onto a 2D plane, we will return to the topic of SMA-based self-folding and demonstrate using physically based modeling methods how the planar "unfolded" shape can be thermally driven to return to the 3D form.

3. Multi-Panel Unfolding

Figure 2: This convex shape is constructed with laser cut poster-board multi-panel papers assembled with brass fasteners.

Our initial goal was to identify a basic mathematical framework for converting any given polygonal mesh surface into a physical structure that is easy to construct. The concept of the "band decomposition" from Topological Graph Theory provides such a basic mathematical framework that helped us to develop a simple multi-panel unfolding method. Band decomposition is obtained by 2D-thickening the graph within the surface and is always contractible to the original graph. In a 2D-thickening, each vertex thickens to a polygon (or a disk) and each edge thickens to a band (See Figure 3). Thus, each polygon corresponds to a vertex and each band corresponds to an edge that connects vertex regions. In the multi-panel method, we convert each vertex of the graph into a star-shaped panel. Edges of the graphs are converted to connectors (i.e., "flaps"). Using this method, we are able to unfold any given polygonal mesh into a set of planar panels, each coming from a vertex of polygonal mesh. We then assemble the panels by connecting corresponding flaps to build large structures. In other

words, the multi-panel unfolding method simply converts each vertex of a graph that is embedded on a surface into a star shaped planar panel. By connecting and folding these panels one can construct a close approximation of the desired surface.

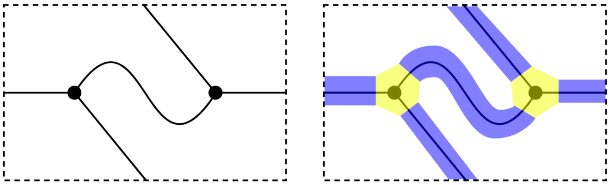

Figure 3: An example of the 2D-thickening in topological graph theory. A graph G in a torus and the associated 2D-thickening.

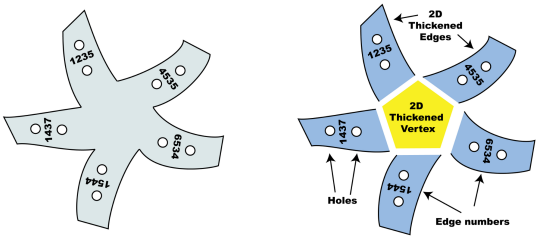

(a) Vertex components (VC) (b) Elements of VC

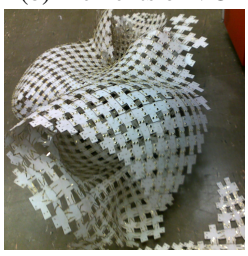

(c) Fasteners (d) Assembling VCs

Figure 4: Construction elements. (a) is an example of a vertex component that is cut with laser cutter, (b) shows elements of a vertex component, which includes a convex shape that corresponds to 2D thickening of the vertex and a set of quadrilateral shaped "flaps" that correspond to 2D thickening of the edges. The flaps are connector parts that are connected by using fasteners that are shown in (c), while (d) is a photograph taken during the process of assembling vertex components with fasteners.

3.1. Motivation for Multi-Panel Unfolding

The multi-panel unfolding is mainly useful for economical and easy construction of large structures. With the design and construction of more and more unusually shaped buildings, the computer graphics community has started to explore new methods to reduce the cost of the physical construction for large shapes. Most of the currently suggested methods focus on reduction in the number of unequally shaped components to reduce fabrication cost. In practice, for operative surfaces incorporating thin metals or thick papers, fabrication is economical even if each component is different. Such operative components can be manufactured fairly inexpensively by cutting large sheets of thin metals or thin paper using laser-cutters, which are now widely available.

One of the biggest expenses for construction of large shapes comes from handling and assembling the large number of components. This problem is analogous to the assembly of a large puzzle. However, while puzzles are intended to be difficult, we seek to simplify the construction process in such a way that the components can be assembled with minimum instruction to the sculptors or builders, who may not have extensive experience.

Note that multi-panel unfolding is not particularly useful for self-folding active materials except where locomotion and self-assembly of structures is possible. Multi-panel does however provide a basic framework that can be extended into self-folding applications.

3.2. Theoretical Framework for Multi-Panel Unfolding

With multi-panel unfolding, we automatically create operative components that can easily be assembled from any given manifold mesh (see Figure 2). This method is based on classical *Graph Rotation Systems* (GRS) [17]. Each operative component, which we call a vertex component, is a physical equivalent of a rotation at the vertex v of a graph G. Each vertex component is a star shaped polygon that corresponds to cyclic permutation of the edge-ends incident on v (See Figure 4(a)). Each vertex component consists of two parts: (1) a convex planar shape that correspond to 2D thickening of the vertex and a set of edge-ends which are actually "flaps". These flaps are quadrilateral shaped operative surfaces with curved boundaries that correspond to 2D thickening of the edges (See Figure 4(b)). 2D vertex components are obtained by unfolding these operative 3D vertex components. The flaps of 2D vertex components are used to assemble the final shape by connecting vertex components with each other. For connecting two vertex components that share an edge, we simply join their corresponding flaps. These can be done either by gluing flaps or by connecting with fasteners as shown in Figure 4(c). We engrave edge-numbers with laser-cutters directly on flaps (edge-ends) of vertex components to simplify finding corresponding edge ends. When we print edge-numbers, we actually define a collection of

rotations, one for each vertex in G. This is formally called a *pure rotation system* of a graph.

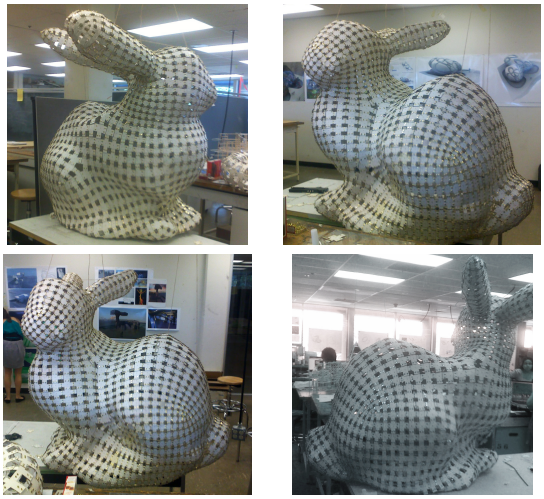

Figure 5: This large sculpture of Bunny is constructed with laser cut poster-board papers assembled with brass fasteners.

Assembly of these panels to construct large structures is based on the fundamental Heffter-Edmunds theorem of GRS. The theorem asserts that there is a bijective correspondence between the set of pure rotation systems of a graph and the set of equivalence classes of embeddings of the graph in the orientable surfaces. As a direct consequence of the theorem, to assemble the structure, the builder must simply attach the corresponding edge-ends of vertex components. Once all the components are attached to each other, the whole structure will correctly be assembled.

This construction guarantees preservation of the local and global Gaussian curvature characteristics of the original surface, resulting in a close approximation of the shape of the surface . Gaussian curvature is an extremely useful measure for shape and structure of surfaces since it relates topology and geometry of the surface through the Gauss-Bonnet Theorem, which implies that for a manifold mesh $\mathcal{M}$, the total Gaussian curvature must be equal to 2π times $\chi(\mathcal{M})$, the Euler characteristic of the corresponding surface [18, 19, 20]. For instance, for a genus-0 manifold mesh, this sum must be equal to 4π. On the other hand, for genus-1 surfaces, the Euler characteristic is zero; therefore, the face-defects must sum to 0.

Since the structure is composed of only operative components, Gaussian curvature is zero everywhere on the solid parts. The Gaussian curvature happens only in empty regions that are determined uniquely. Since, we correctly form Gaussian curvature of holes, the structures will always be raised and formed in 3-space, closely approximating the overall shape of the initial surface.

We convert polygonal meshes to sculptures that are composed of operative vertex components. In polygonal meshes, we use discrete versions of Gaussian curvatures. Discrete Gaussian curvature for vertexes of triangular (or planar) meshes is known as a vertex defect and for every vertex of piecewise planar meshes [21, 22, 23], it is defined as

$$\Theta = 2\pi - \textstyle\sum_{i=0}^{n-1} \theta_i \tag{3.1}$$

where θ_i is the angle at corner i of the vertex and n is the valence of the vertex.

The resulting sculptures represent the dual of the original polygonal mesh. Therefore, the faces (i.e. holes) of the sculpture correspond to the vertices of the original mesh. On the other hand, the vertices of the sculpture (vertex components) correspond to the faces of the original mesh. Note that the faces of original mesh are either planar or approximately planar. It is therefore easy to create the vertex components, which can be fabricated with developable materials such as paper or thin metal. When we use developable materials, if there is no deformation (regardless of the level of component bending), the Gaussian curvature is zero [22]. In other words, Gaussian curvature happens only at the holes of the final sculptures. Since these holes correspond to vertices of original polygonal mesh, the Gaussian curvature of any hole must correspond discrete Gaussian curvature of its corresponding vertex in the original polygonal mesh.

Note that Discrete Gaussian curvature for a face is known as a face defect [20, 24], and is defined as

$$\Phi = \sum_{j=0}^{n} \phi_j - (n-2)\pi \tag{3.2}$$

where ϕ_j is the angle at corner j of a hole and n is the number of the sides of the hole. The Gaussian curvature for holes will also be computed the same way. To make Gaussian curvature of every hole Φ equal to Θ of its corresponding vertex in the original mesh is straight forward. Let ϕ_i and θ_i be two corresponding corners of a hole in the sculpture and its corresponding vertex in the original mesh. If we choose $\phi_i = 2\pi - \theta_i$, then $\Phi = \Theta$ for such corresponding hole-vertex pair. We use this property to create vertex components.

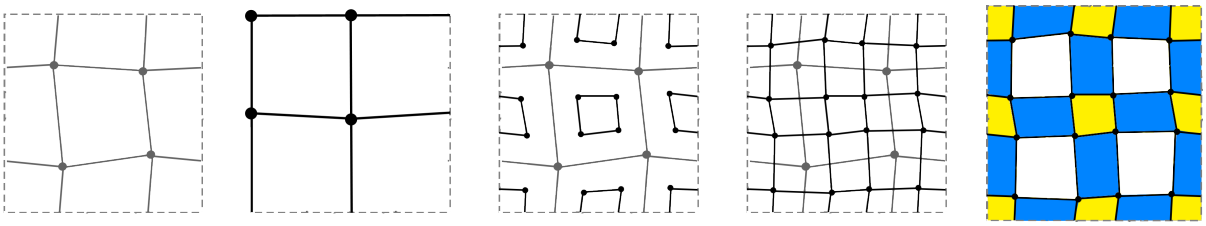

(a) Toroidal Mesh (b) Dual Graph (c) Thickened Vertices (d) Adding Connectors (e) Color Coded View

Figure 6: The basic algorithm for 2D thickening: (a) shows a toroidal mesh surface M. (b) shows the dual graph that is obtained by creating a vertex for every face of the mesh M and by inserting an edge between every two neighboring vertices. (c) shows faces obtained by scaling the original faces of the polygonal mesh. This operation corresponds to the 2D-thickening of the vertices of the dual graph. (d) shows the adding connectors between thickened vertices. (e) shows the result that corresponds to 2D thickening of dual graph. The yellow faces in are 2D thickened vertices and blue faces are 2D thickened edges of the dual graph. White regions are holes.

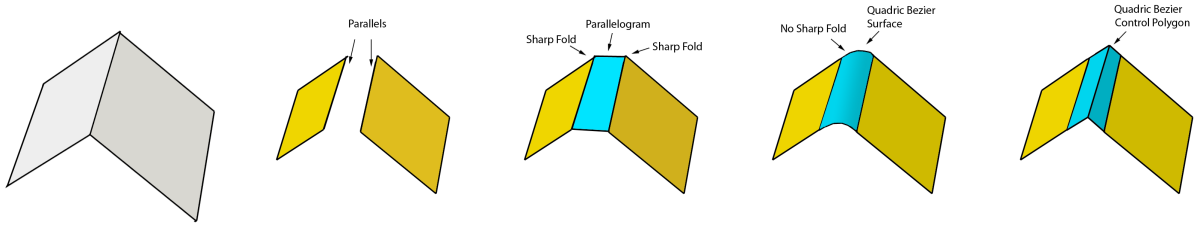

(a) Two Neighboring Mesh Faces (b) Thickened Vertices i.e. Scaled Faces (c) Thickened Edge Planar Paralellogram (d) Thickened Edge Bezier Surface (e) Bezier Control Polyhedron

Figure 7: Vertex and edge thickening process. (a) shows two neighboring faces that correspond to two vertices of dual graph that is connected by an edge. (b) shows scaled faces that correspond to thickened vertices. Note that scaling guarantees production of edges that are parallel to each other. (c) shows simple edge thickening that is obtained by connecting the two parallel edges of scaled faces. Note that this operation creates sharp folds. (d) shows the thickening we use: a quadric Bezier surface. This connector does not have sharp folds. Moreover, it is developable and has zero Gaussian curvature. (e) shows the control polygon of the quadric Bezier connector.

3.3. Implementation

We have developed software that automatically creates and draws the shapes of assembly-ready vertex components from any given polygonal mesh. Our goal is to obtain developable or piecewise planar 3D vertex components such that they can be unfolded to a plane with no distortion. For this purpose, we first convert an initial polygonal mesh into mesh with planar and convex faces. Such a mesh can always be obtained by triangulating all the faces of the initial mesh. On this piecewise-planar surface, there always exists a dual graph that can be obtained by creating a vertex for every face of the polygonal mesh and by inserting an edge between every two neighboring vertices. Figure 6(b) shows the dual graph on a surface as shown in Figure 6(a). Our implementation provide 2D thickening of these dual dual graph embedded on planar mesh surface. There are three advantages of this approach: (1) The neighborhoods of the vertices of the dual graph to a planar mesh are always planar. Therefore, vertex thickening always provide a planar polygon. (2) Vertex thickening always result in a convex planar polygon that is obtained by scaling the original faces of planar mesh (See Figure 7(a) and (b)). (3) Edge thickening can always result in simple planar or developable surfaces (See Figure 7(c) and (d)). Note that this process is closely related to a corner-cutting operation [25], which is the remeshing scheme of Doo-Sabin subdivision [26].

Using the smart materials laminates, it is considered herein difficult to obtain “sharp” folds. Therefore, in our implementation employs Bezier connectors to avoid sharp folds. We approximate Bezier connectors with a set of planar parallelograms. To obtain each vertex component, we simply unfold each Bezier connector into the plane of its thickened vertex. This process result in panels that are similar to vertex components shown in Figure 4. Each of these planar star shaped polygons can be cut with laser cutter. These panels guarantee that a close approximation of the initial mesh surface can be constructed.

In summary, there are three properties of our vertex components that allow one to obtain a developable sculpture that is a close approximation of initial man-

ifold mesh surface:

(1): The vertex components are guaranteed to be developable. Therefore, they can easily be unfolded. Moreover, after the construction of the shape Gaussian curvature is zero everywhere except at the holes.

(2): The method guarantees that the Gaussian curvature of any hole resulting from construction provides a discrete Gaussian curvature identical to that of the corresponding vertex in the original polygonal mesh. This property guarantees that the shape of the sculpture will closely resemble the shape of the original polygonal mesh.

(3): Since Gaussian curvature directly comes from the original polygonal mesh, the total discrete Gaussian curvature over the whole sculpture is equal to total discrete Gaussian curvature of the original polygonal mesh, which is the product of the Euler characteristics with 2π. This property guarantees that the sculpture will be closed without any deformation.

3.4. Physical Construction

Using our custom software, we have first converted simpler polygonal meshes such as Archimedean solids into paper sculptures as shown in Figure 2. We have also built toroidal surfaces (not shown). Our initial experiments showed that one of the problems for builders is the location of desired components from a large number of pieces. To simplify the process, we have also developed strategies for easily finding corresponding pieces among a large number of vertex components. Using this approach, architecture students have constructed a large version of the Stanford Bunny (see Figure 5) in a design and fabrication course in College of Architecture. The costs of poster-board papers and fasteners were minimal (less than $100). Multi-panel unfolding method can be especially effective in constructing larger shapes when using stronger materials. The structures obtained by this method can also be used as molds to cast large plaster or cement sculptures. However, for self-assembled materials, manual fasteners would not be appropriate. To use multiple panels, there is a need for automatic assembly. In this current work, we will avoid self-assembly and will instead focus on a single-panel unfolding method that does not require the assembly of multiple panels.

4. Single-Panel Unfolding

Shape memory alloys are materials capable of providing substantial shape changes under the imposition of high loads when sufficiently heated. We will eventually fabricate planar structures from sheets that include these shape memory alloys. When these planar structures are heated locally and to the proper extent, they will form a desired shape without any need for manual assembly. Multi-panel structures, being assembled using additional elements such as fasteners or glue, clearly require such manual assembly. This self-assembly problem will be addressed in future works considering: (1) development of different latching ideas and (2) creation of complicated assembly maneuvers in 3-space via controlled heating sequences. In this paper, however, we focus on single-panels without connection flaps. There will be no separate vertex components and all thickened vertices will be connected by a subset of connecters, which we call hinges. The main constraint of single-panel unfolding is that one can only consider convex shapes, which can be unfolded into a simple (i.e., non-self-intersecting) 2D polygon. Assuming that the desired 3D shape is convex, the algorithm to obtain single-panel unfolding is a straightforward extension of the multi-panel unfolding scheme.

4.1. Algorithm

Our algorithm for single-panel unfolding consists of five steps:

(1) Triangulate: Since the initial mesh may not necessarily be planar, we first triangulate any non-triangular faces to guarantee that every face is planar. This step is skipped if the mesh is already triangulated or if the faces are already planar and convex. In our current implementation, we triangulate non-triangular faces even when they are planar and convex. This results in a fully triangular mesh as shown in Figure 8(a) and Figure 9(a).

(2) Construct Dual Graph: In this stage, we construct a dual graph from the mesh using the dual mesh in which every original face becomes a vertex and every original vertex becomes a face [27]. The dual graph is a graph that consists of the edges and the vertices of the dual mesh.

(3) 2D-Thicken a Spanning Tree of Dual Graph: A spanning tree is a tree that includes all vertices of a given graph [28]. If we 2D-thicken a spanning tree, the result will be one single panel formed in 3D as shown in shown in Figures 8(b) and 9(b). In this case, every vertex of the dual graph will be 2D-thickened into a triangle and every edge of the spanning tree will be 2D-thickened into a developable quadrilateral. Note that these edges now are not free-floating "flaps", but rather

"connectors" that do not require assembly. Therefore, any spanning tree of the dual graph corresponds to a single-panel solution. We simply choose one of many possible spanning tree of the dual graph to obtain one possible single-panel solution. The particular structures shown in Figures 8(b) and 9(b) are appropriate for the finite element analysis considered herein. If we want to assemble these shapes manually, flaps are required. To obtain flaps, the half-edges that are not part of spanning tree are 2D thickened. Examples of 2D thickened spanning trees with flaps are are shown in Figure 10. These shapes have been manually constructed by gluing flaps.

(4) Unfold: Since the 2D thickened spanning trees consist of only planar and developable components with smooth physically realistic curvatures, it is easy to unfold them into 2D planar shapes as shown in Figures 8(c) and 9(c). Again note that these particular shapes do not have flaps since they are created for finite element analysis. For manual construction, we also include flaps as shown in the left column of in Figure 10.

(5) Refine: In finite element analysis (FEA), it is important to consider the effect of mesh refinement on analysis accuracy. Straightforward unfolding results in relatively simple linear elements for FEA. Therefore, a refinement process that provides higher number of elements is needed to properly prepare the planar domain for re-folding analysis. To this end, we subdivide the 2D polygon into a 2D polygonal mesh that can more accurately be simulated in FEA software as shown in Figures 8(d) and 9(d). We particularly refine the mesh in the areas of folding (i.e., the areas of physically interesting behavior).

This algorithm guarantees to create a single-panel regardless of the shape of the initial mesh and the choice of the spanning tree. However, unfolded single panels can be self-intersecting. This is not desired since we want to cut the panels from a single sheet. Therefore, we also need to guarantee that single panels will not non-self-intersect.

To obtain non-self-intersecting single-panels, all vertices of original polygonal mesh must have a positive vertex defect, (i.e., positive Gaussian curvature). In other words, the shape of the initial polyhedral mesh must be convex. The spanning tree can be selected randomly.

The problem with non-convex shapes is that they can have saddle points, in which the Gaussian curvature is negative. In other words, there exist at least one vertex of original polygonal mesh with negative vertex defect in non-convex shapes. It is not possible to unfold a negative-defect vertex without self intersection. One possible idea can be to use vertex split operation [27]. This can remove local self-intersections caused by negative curvature while global self-intersections may remain.

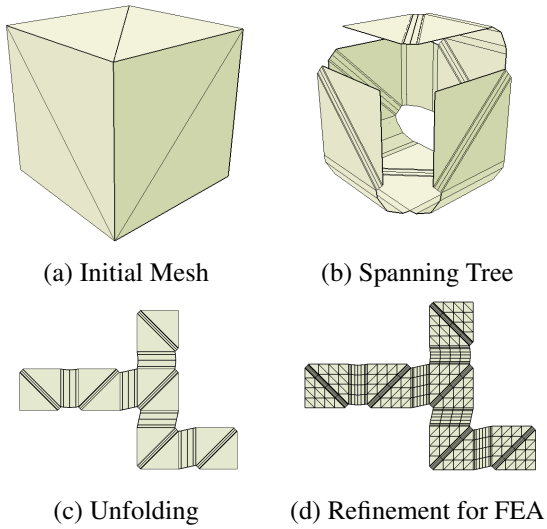

(a) Initial Mesh (b) Spanning Tree

(c) Unfolding (d) Refinement for FEA

Figure 8: The procedure to obtain a single-panel unfolding from a cube.

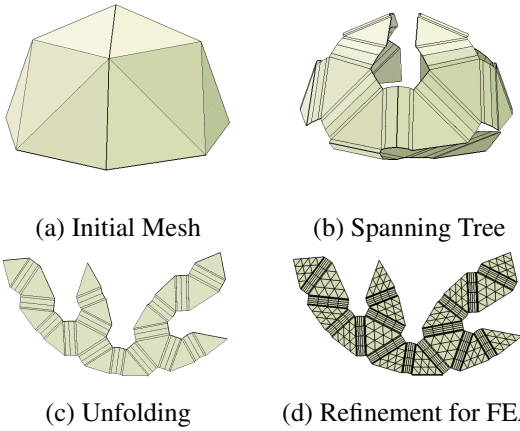

(a) Initial Mesh (b) Spanning Tree

(c) Unfolding (d) Refinement for FEA

Figure 9: The procedure to obtain a single-panel unfolding from a dome.

4.2. Implementation

We have extended our multi-panel unfolding software to handle single-panel unfolding. The software randomly selects one spanning tree. Using this spanning tree, it creates a developable form that is a 2D-thickened version of the selected spanning tree. It also unfolds and

draws the shape of the single panel. The software works for any given polygonal mesh, convex or not. If the initial mesh is not convex, a single panel is still generated though such a single panel is not physically realizable since it will self-intersect. Our single-panel unfolding again guarantees a close developable approximation to the initial mesh surface. We have manually assembled a few examples as shown in Figure 10 by gluing corresponding flaps to qualitatively compare resulting shapes with finite element analysis.

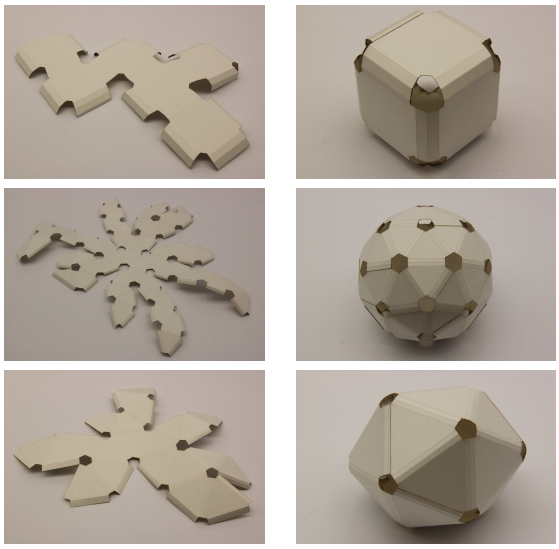

Figure 10: Examples of shapes constructed from single-panels.

4.3. Computational Evaluation: Finite Element Analysis

The goal of the computational evaluation component of this research is to determine via physically based methods how a laminate sheet composed of two thin SMA layers sandwiching a third passive and compliant (i.e., elastomeric) layer might be thermally induced to self-fold at multiple pre-selected areas. The 3-layer material laminate configuration is shown in Figure 11. The coordinated self-folding is performed such that an original form, "unfolded" to a planar configuration via the algorithm in Section 4.1, can be "re-folded" into that form once again. Here the computational evaluation of the self-morphing sheet response was performed using an analysis framework for shape memory alloy structures commonly applied to morphing aerospace applications [29], which includes the numerical implementation of mathematical material models for the SMA and elastomer layers into a finite element analysis setting. We briefly describe how the physical domain generated by the unfolding algorithm is used to initiate the finite element modeling process, how the shape memory alloy and elastomer regions are modeled, and what physical mechanisms and conditions were considered. Analysis results for two distinct shapes are then provided.

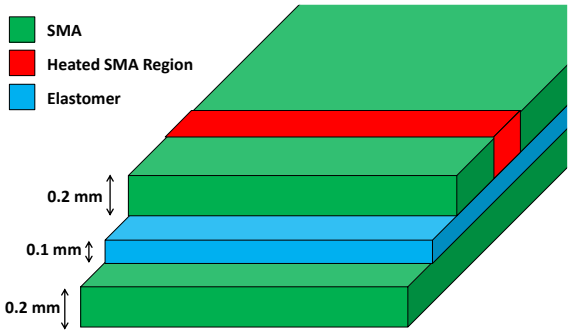

Figure 11: Laminate configuration and dimensions for the studied folding sheet.

4.3.1. The physical domain

The implemented algorithm of Section 4.1 provides as quantitative output the full mesh, including the location of all nodes and the element connectivity. The `.inp` file format used in commercial Abaqus Unified FEA Suite [30] is similar to `.obj` file format (provided by our custom software). Therefore, with a minor change in the `.obj` reader and writer already implemented, we export unfolded single-panel data in `.inp` file format that can be directly read by Abaqus.

In the current implementation, only triangular elements with linear shape functions (`Abaqus type=S3`) and quadrilateral elements with linear shape functions (`Abaqus type=S4R`) are considered. Note that it is straightforward to scale the nodal positions such that the morphing sheet size is readjusted based on real-world intents.

It is further possible for the unfolding algorithm to output sets (formatted lists) of the nodes and associated elements that comprise hinge regions, which are the regions where heat is applied, as well as those that comprise planar regions. This is important in determining which nodes should be subjected to thermally induced actuation in the physical analysis and which should not. FEA preprocessing also includes the definition of thermal histories for the folding regions, the imposition of boundary conditions, body forces (i.e., gravity), contact constraints (i.e., between the folding sheet and a

rigid "floor"), and the assignment of material definitions, which includes the consideration of the unique material behavior of the shape memory alloy.

4.3.2. Material constitutive behavior

If the reference configuration of the morphing sheet is taken to be its planar configuration when fully unfolded, then the displacement vector $\mathbf{u} = \{u_x, u_y, u_z\}^{\mathrm{T}}$ at any given point in the sheet describes the motion of that point throughout the folding process. If the local material extension/compression in the sheet is relatively small at all points, then a material model can be accurately postulated in terms of the so-called *infinitesimal strain* per

$$\boldsymbol{\varepsilon} = \frac{1}{2}\left[(\boldsymbol{\nabla}\mathbf{u}) + (\boldsymbol{\nabla}\mathbf{u})^{\mathrm{T}}\right], \tag{4.3}$$

where $\boldsymbol{\nabla}$ denotes the gradient operator in a material-fixed coordinate system[1]. The general material response of both the shape memory alloy and elastomer lamina that comprise the overall sheet are then formulated in terms of the local strain and its energetic conjugate, the local stress $\boldsymbol{\sigma}$. The process of solving the highly non-linear morphing structural problem via FEA involves an iterative process (often based on Newton's method) [33].

The stress-strain response of the elastomer material layer is described here using a simple linear relation (i.e., Hooke's law) between the strain and stress tensors, given as

$$\boldsymbol{\varepsilon} = \boldsymbol{\mathcal{S}}^{elast}\boldsymbol{\sigma} + \boldsymbol{\alpha}^{elast}(T - T_0), \tag{4.4}$$

where $\boldsymbol{\mathcal{S}}^{elast}$ is known as the *compliance tensor* and $\boldsymbol{\alpha}^{elast}$ is known as the *coefficient of thermal expansion tensor*. Finally, T_0 is a reference temperature and T is the current local temperature.

The behavior of the shape memory alloy, however, is non-linear and history-dependent. A simple linear model will not suffice. The detailed foundation and description for the constitutive model for shape memory alloys used in this study is provided elsewhere [34]. The model focuses on the generation and recovery of *transformation strains* that occur as a results of phase transformation in the material that is both stress- and temperature-induced. Here the discussion is restricted to the analysis of transformation during heating only. Given a known local temperature evolution and the non-linear finite element methodology that utilizes guess strains, the model computes three unknowns (13 total components): $\boldsymbol{\sigma}$, $\boldsymbol{\varepsilon}^t$, and ξ. Analogous to the formulation of the elastomer response given in (4.4), the total strain is assumed to be related to the stress and temperatures per Hooke's law given as

$$\boldsymbol{\varepsilon} = \boldsymbol{\mathcal{S}}^{SMA}(\xi)\boldsymbol{\sigma} + \boldsymbol{\alpha}^{SMA}(T - T_0) + \boldsymbol{\varepsilon}^t, \tag{4.5}$$

where the SMA compliance varies linearly during the phase transformation per

$$\boldsymbol{\mathcal{S}}^{SMA}(\xi) = \boldsymbol{\mathcal{S}}^{A} + \xi(\boldsymbol{\mathcal{S}}^{M} - \boldsymbol{\mathcal{S}}^{A}) = \boldsymbol{\mathcal{S}}^{A} + \xi\Delta\boldsymbol{\mathcal{S}}, \tag{4.6}$$

"A" and "M" denoting the heated and cooled phases of the SMA material, respectively. Comparing (4.5) and (4.4), one notes that the additional contribution to the total strain, $\boldsymbol{\varepsilon}^t$, must now be computed. This recoverable transformation strain drives the self-morphing and evolves such that the time rate of change of both its magnitude and direction are given per the following (when heating):

$$\dot{\boldsymbol{\varepsilon}}^t = \dot{\xi}\boldsymbol{\varepsilon}^{t-r}; \quad \dot{\xi} < 0, \tag{4.7}$$

where $\boldsymbol{\varepsilon}^{t-r}$ is the transformation strain tensor at the beginning of actuation. Here we assume that this is the maximum recoverable strain the material is capable of providing and that the SMA has been strained to this level during fabrication (i.e., prior to being bonded to the elastomer). During heating ($\dot{\xi} > 0$), the direction and magnitudes are defined such that all transformation strain existing in the SMA lamina after fabrication (i.e., in the unfolded configuration) is fully recovered when the SMA material is heated to the completion of transformation.

The constraints on the evolution of martensitic volume fraction ξ must also be defined. To this end, the transformation constraint function $\Phi^t(\boldsymbol{\sigma}, T, \xi)$ is introduced and we have

$$\Phi \leq 0, \qquad \dot{\xi}\Phi = 0, \qquad 0 \leq \xi \leq 1, \tag{4.8}$$

where, if the discussion is restricted to heating only

$$\begin{aligned} \Phi = \Phi_{rev} &= -(1+D)\boldsymbol{\sigma} : \boldsymbol{\varepsilon}^{t-r} - \tfrac{1}{2}\boldsymbol{\sigma} : \Delta\boldsymbol{\mathcal{S}}\boldsymbol{\sigma} \\ &+ \rho\tilde{u}_0 - \rho\tilde{s}_0 T - Y_0 \\ &+ [\tfrac{1}{2}a_2(1 + \xi^{n_3} + (1-\xi)^{n_4}) - a_3]. \end{aligned} \tag{4.9}$$

The constitutive model can then be summarized as follows: given a loading history in terms of $\boldsymbol{\varepsilon}$ and T, the transformation strain $\boldsymbol{\varepsilon}^t$ is evolved using (4.7), where the stress-strain coupling is described by (4.5) and the

[1] The effect of arbitrarily large local rotations such as those observed during the folding process has been satisfactorily accounted for even for this "small strain" assumption using the algorithm of Hughes and Winget [31, 32].

constraints on the evolution of the martensitic volume fraction ξ are presented in (4.8).

To utilize the material models for both the SMA and the elastomer, material property values must be established. Neglecting the coefficient of thermal expansion (i.e., $\boldsymbol{\alpha}^{elast} = \boldsymbol{\alpha}^{SMA} = \mathbf{0}$), the thermoelastic response of both materials can be described by properly populating their respective compliance tensors. Assuming that the SMA and elastomer are *isotropic* (i.e., their elastic responses are independent of the direction of deformation) [35], the components of $\boldsymbol{\mathcal{S}}$ are given in terms of the two conventional material properties *Young's modulus* or extensional stiffness (E), and the *Poisson's ratio* or ratio of transverse deformation to axial deformation during uniaxial extension (ν) [35].

The unique behavior of the SMA is further described by the initiation of six components of $\boldsymbol{\varepsilon}^{t-r}$ and by the following 10 scalars that describe the transformation criteria: $\rho\Delta s_0$, $\rho\Delta u_0$, a_2, a_3, Y_0, D, n^1, n^2, n^3, and n^4. These will be provided in the following subsection.

4.3.3. Analysis results

In the current computational study, a dynamic analysis was performed to assess the thermally induced actuation of the morphing sheets while considering such aspects as inertia on the motion of the individual panels. Further, the effects of gravity are considered in the model, which requires the modeling of a rigid surface (i.e., a "table") on which the self-folding sheets rest. Specifically, the gravitational constant is taken to be $g = 9.81\ \mathrm{m/s^2}$, and the interfaces between the sheets and the rigid surfaces are taken to be frictionless. In order to avoid unconstrained in-plane motion, a point in the structure is set to have zero displacement in the in-plane directions. This idealization will not be necessary when we model friction between the sheets and the rigid surfaces in future work. Finally, the material properties of both the elastomer and SMA layers needed to complete the analysis, including the density ρ, are given in Table 1 and Table 2, respectively. Note that these properties are quite common.

In summary, the following inputs are needed in order to perform FEA of the folding sheets:

- Mesh parameters: initial node locations, node connectivity, and hinges heating regions node sets (from `.obj` file provided by our custom software).
- Material properties (from selected materials).
- Laminate layer thicknesses (from folding sheet design [15]).
- Boundary conditions and applied fields: interactions with other bodies, gravity, etc. (application dependent).
- Heating rate and maximum applied temperature (from iterative trial simulations with the objective of setting the desired final configuration at a prescribed final time).

Table 1: Material properties for the elastomer layer.

Material Property	**Value**
ρ^{elast}	$3000\ \mathrm{kg/m^3}$
E^{elast}	100 MPa
ν^{elast}	0.45

Table 2: Material properties for the SMA layers.

Material Property	**Value**
ρ^{SMA}	$6450\ \mathrm{kg/m^3}$
$E^A,\ E^M$	70000 MPa, 30000 MPa
$\nu^A = \nu^M$	0.33
$\varepsilon_1^{t-r} = \varepsilon_2^{t-r},\ \varepsilon_3^{t-r}$	0.025, -0.050
$\rho\Delta s_0,\ \rho\Delta u_0$	-0.519 $\mathrm{MJ/m^3}$, -157 $\mathrm{MJ/m^3}$
$a_2,\ a_3$	5.19 $\mathrm{MJ/m^3}$, 0 $\mathrm{MJ/m^3}$
$Y_0,\ D$	5.19 $\mathrm{MJ/m^3}$, 0 $\mathrm{MJ/m^3}$
$n^1 = n^2 = n^3 = n^4$	0.8

The finite element analysis results for the self-folding morph toward a cube shape are shown in Figure 12, while those for self-folding toward a dome shape are shown in Figure 13. The cube form was selected for both its common, classical shape and the necessity for 90° folds. The choice of the dome was inspired by engineering and architectural motivations that consider a self-assembling habitation for such purposes as space exploration or high-mobility humanitarian activities. Recall that morphing is induced by selectively heating the hinge regions from room temperature to locally-defined higher temperatures. The locally-defined temperature at the hinges varied linearly with respect to time. The maximum temperature applied at the hinges was determined by means of trial and error simulations with the objective of setting the desired final configuration at a prescribed final time.

The FEA results illustrate the deformation of the sheets as they morph toward their final shapes, while the contours indicated the degree to which local regions have transformed from initially 100% cold phase (martensite) toward 100% hot phase (austenite). Full transformation is not necessary as this would lead to excessive curvature in the fold regions and thus distorted forms. According to this analysis, it is in fact feasible to consider that self-folding sheets could be fabricated with sufficient strain and strength to lift their own weight and sufficient strain (deformation) to complete a morphing process from a flat sheet to a predetermined three-dimensional shape.

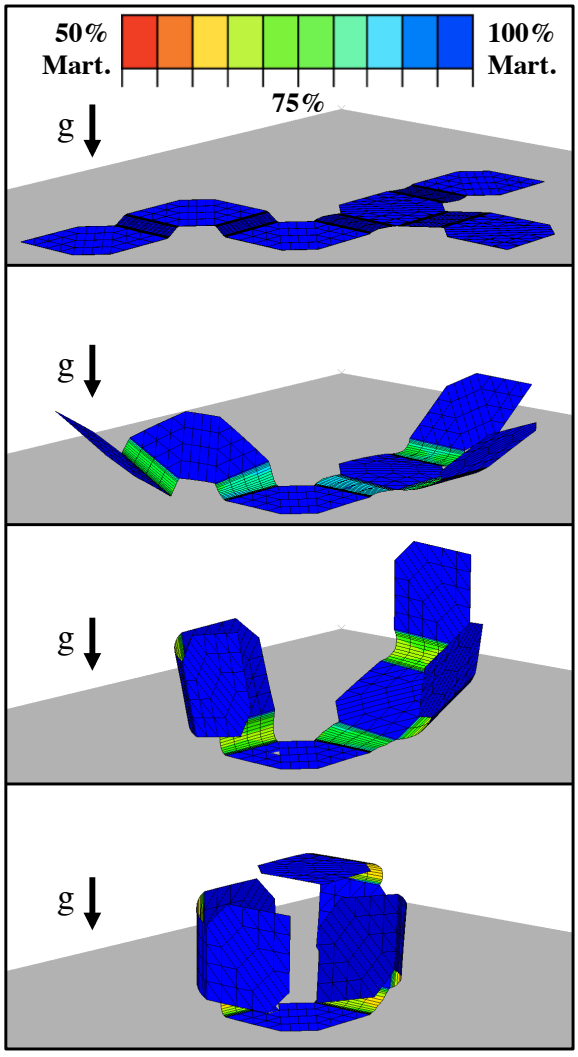

Figure 12: Analysis results considering the thermally induced morphing of an SMA-based laminate sheet configured to self-fold into a cube structure. Contour plot indicates local phase transformation progress.

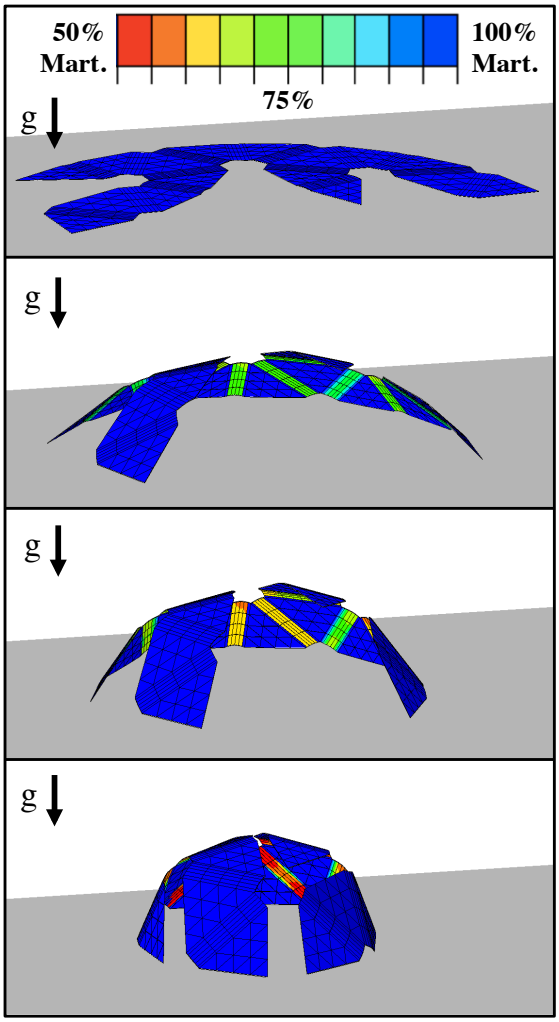

Figure 13: Analysis results considering the thermally induced morphing of an SMA-based laminate sheet configured to self-fold into a dome structure. Contour plot indicates local phase transformation progress.

The power of this modeling technique goes beyond the deformed contour plots of Figure 12 and Figure 13. Quantitative results can also be assessed, such as the maximum and minimum transformation required over all fold regions as shown in Figure 14. As indicated by the non-uniform fold coloring in the contour plots, although they are homogeneously heated, all fold regions do not experience the same amount of phase transformation. This is especially due to the formulation of (4.9), which couples stress and temperature such that folds with higher stresses (i.e., those lifting panels against the force of gravity) experience less transformation even at the same temperature condition. Further, the folding of cube panels at first against and then in the direction of

gravity leads to a highly non-linear evolution in local fold stress as the morphing process evolves, and this can be seen in Figure 14. Understanding these relationships, the actuation requirements, and the capabilities of the important folding regions will be essential in fabricating and utilizing the self-folding structures proposed herein.

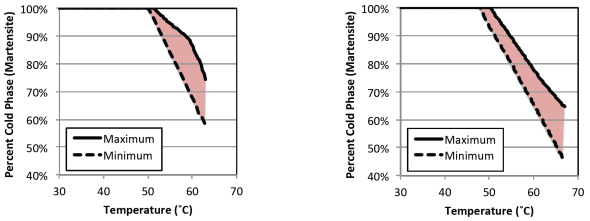

(a) Cube model (b) Dome model

Figure 14: Evolution of maximum and minimum cold phase (martensite) fraction in the fold regions with increasing fold temperature. Note the physical non-uniformity.

5. Discussion and Additional Results

In the FEA simulations, we removed the flaps to avoid complex connections. The connections are needed, however, to keep the shape in the desired form without need for permanent heating. If connections are not present, removal of localized hinge heating will return the 3D form back to its planar shape. Our current methods for assembly, fastening, or gluing are not good options since they require manual intervention. We are currently working on three schemes for connecting flaps: (1) Magnetized flaps, (2) Flaps that have slits in the middle, and (3) Flaps that can hook each other.

Magnetized flaps: The artistic representation given in Figure 1 shows an example shape that can be used for magnetized flaps. Such flaps can automatically be assembled once two corresponding flaps come sufficiently close to each other. Despite the clear advantages, we expect these types of flaps will present a manufacturing challenge. In current case, we assume that the whole panel is cut from the same material, which is a simple process. The inclusion of magnetized flaps would require that we determine how to magnetize local panel regions.

Flaps with slits: Such flaps would consists of two parts that are slitted in the middle [36, 37] (See Figure 15a). When the two corresponding flaps come closer, each flap will be heated in such a way that alternate flaps go

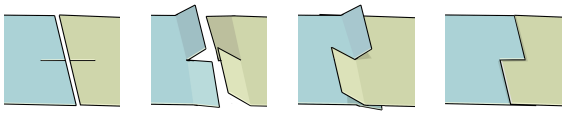

(a) (b) (c) (d)

Figure 15: Flaps that have slits in the middle. These flaps can easily be assembled just by sliding appropriately shaped flaps into each other. On the other hand, they are not tightly locked.

in alternate directions (up and down) (See Figure 15b). This heating will create two pieces that can slide together easily (See Figure 15c). Once the shape is formed, these flaps will be locked by friction (See Figure 15d). The advantage of this approach is that the heating control will be simple. On the other hand, the connection may not be that strong since the flaps do not have any rigid connection mechanism.

Slitted flaps with hooks: These flaps will, in essence, be similar to simple flaps with slits, but they will have additional hooks that can allow the two pieces to tightly locked (See Figure 16a). The lock created by this mechanism will be stronger than the two previous proposed approaches. On the other hand, the maneuvers needed to obtain the lock will be complicated (See Figure 16b and c) and the operation will require complex heating strategies to obtain desired maneuvers.

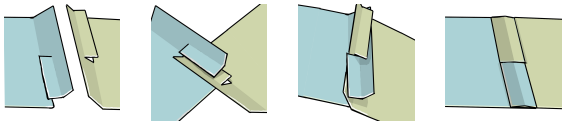

(a) (b) (c) (d)

Figure 16: An example of flaps that can hook each other. These flaps can be locked better than flaps with slits in the middle. On the other hand, the assembly of such flaps require complex maneuver in 3D space.

We have extended our single-panel unfolding software to obtain flaps. One minor problem with flaps is that flaps of unfolded single panels can be self-intersected even when initial shape is convex. To avoid this problem we use two strategies: (1) Instead of choosing the spanning tree randomly, we start from high positive curvature regions which makes flaps as away from each other as possible and (2) we use smaller flaps. Using this approach, we have build a few objects using single panels with slitted flaps. Although the resulting paper structures are not as stable as fastened or glued structures, even simple slits improves the stability of the structures significantly.

6. Conclusion and Future Work

In this paper, we have demonstrated that it is possible to form desired shapes by appropriately heating planar single panel sheets made from shape memory alloy-based laminates. There is significant future work needed to be done in order to effectively synthesize complex structures from programmable self-folding active materials for real-world applications.

One major issue with single-panel unfolding method is that it can only support convex shapes. A general shape can be decomposed into convex shapes, but the number of convex components can be large. A solution to this problem is to decompose the shape with approximate convex components [38, 39]. We also explore Morse-Snell decomposition methods such as [40] to obtain approximate convex components. Each of these approximately convex components can be turned into a closest convex mesh and these convex components will form a map on the surface, which can be represented as a graph where each vertex of the graph corresponds to a convex component and each edge of the graph corresponds a border shared by two components. From this graph, we can again form a spanning tree. If we connect the panels only in one point that is given by a selected spanning tree, the whole system of convex components can be unfolded to a plane. Each convex component can be unfolded into a single planar panel and these panels can be manually connected using fasteners. One advantage of this approach is that the resulting shape will be planar, but consisting of overlapping pieces.

Another issue will be the reduction of the overall footprint of unfolded panels. In some cases, it may be wise to allow overlapping panels to reduce the total footprint of unfolded panels. However, allowing overlapping panels will require more complicated folding procedures and heating strategies.

Finally, shape memory alloys allow controlled localized deformation of regions where heat is applied. Using this property, an additional future effort will be the exploration of direct manipulations of Gaussian curvature to form desired shapes.

References

[1] R. Lang, Origami: Complexity in creases (again), Engineering and Science 67 (1) (2004) 5–19.

[2] K. Miura, Triangles and quadrangles in space, Proceedings of the International Association for Shell and Spatial Structures (IASS) Symposium 2009 (2009) 27–38.

[3] E. Demaine, J. O'Rourke, Geometric Folding Algorithms: Linkages, Origami, Polyhedra, Cambridge University Press, Cambridge, 2007.

[4] E. D. Demaine, J. O'Rourke, Geometric Folding Algorithms: Linkages, Origami, Polyhedra, Cambridge University Press, New York, NY, USA, 2008.

[5] J. O'Rourke, How to Fold It: The Mathematics of Linkages, Origami, and Polyhedra, Cambridge University Press, Cambridge, 2011.

[6] T. Tachi, Origamizing polyhedral surfaces, IEEE Transactions on Visualization and Computer Graphics 16 (2) (2010) 298–311.

[7] J. Mitani, H. Suzuki, Making papercraft toys from meshes using strip-based approximate unfolding, ACM Trans. Graph. 23 (3) (2004) 259–263.

[8] K. Otsuka, C. M. Wayman (Eds.), Shape Memory Materials, Cambridge University Press, Cambridge, 1999.

[9] A. V. Srinivasan, D. McFarland, Smart Structures: Analysis and Design, Cambridge University Press, Cambridge, U.K., 2000.

[10] E. Hawkes, B. An, N. Benbernou, H. Tanaka, S. Kim, E. Demaine, D. Rus, R. Wood, Programmable matter by folding, Proceedings of the National Acadamies of Science 107 (28) (2010) 12441–12445.

[11] K. Kuribayashi, K. Tsuchiya, Z. You, D. Tomus, M. Umemoto, T. Ito, M. Sasaki, Self-deployable origami stent grafts as a biomedical application of ni-rich tini shape memory alloy foil, Materials Science and Engineering: A 419 (1,2) (2006) 131–137.

[12] Y. Liu, J. K. Boyles, J. Genzer, M. D. Dickey, Self-folding of polymer sheets using local light absorption, Soft Matter 8 (6) (2012) 1764–1769.

[13] P. Krulevitch, A. P. Lee, P. B. Ramsey, J. C. Trevino, J. Hamilton, M. A. Northrup, Thin film shape memory alloy microactuators, Journal Of Microelectromechanical Systems 5 (4) (1996) 270–282.

[14] M. Tomozawa, H. Kim, S. Miyazaki, Shape memory behavior and internal structure of TiNiCu shape memory alloy thin films and their application for microactuators, Acta Materialia 57 (2) (2009) 441 – 452. doi:10.1016/j.actamat.2008.09.026.

[15] D. Hartl, K. Lane, R. Malak, Computational design of a reconfigurable origami space structure incorporating shape memory alloy thin films, Proceedings of SMASIS12: ASME Conference on Smart Materials, Adaptive Structures and Intelligent Systems, September 19–21, 2012, Stone Mountain, GA (2012) 1–9.

[16] E. Peraza-Hernandez, D. Hartl, R. Malak, Simulation-based design of a self-folding smart material system, Proceedings of IDETC/CIE 2013: ASME International Design Engineering Technical Conference & Computers and Information in Engineering Conference, August 4–7, 2013, Portland, OR (2013) 1–9.

[17] J. L. Gross, T. W. Tucker, Topological Graph Theory, Wiley Interscience, New York, 1987.

[18] T. Watkins, Gauss-Bonnet Theorem and its Generalization, http://www.applet-magic.com/gaussbonet.htm, 2011.

[19] E. W. Weisstein, Gauss-Bonnet Formula, From MathWorld–A Wolfram Web Resource,http://mathworld.wolfram.com/Gauss-BonnetFormula.html, 2013.

[20] E. Akleman, J. Chen, Practical polygonal mesh modeling with discrete gauss-bonnet theorem, in: Proceedings of Geometry Modeling and Processing (GMP'06), 2006, pp. 287–298.

[21] D. Huffman, Curvature and creases: A primer on paper, IEEE Transactions on Computers 25 (10) (1976) 1010–1019.

[22] C. R. Calladine, Theory of Shell Structures, Cambridge University Press, Cambridge, 1983.

[23] M. M. Etal, Discrete differential-geometry operators for trian-

gulated 2-manifolds, in: in H.-C. Hege and K. Polthier eds, Visualization and Mathematics III, Springer, 2003, pp. 35–57.
[24] E. Akleman, J. Chen, J. L. Gross, Paper-strip sculptures, Shape Modeling and Applications, International Conference on (2010) 236–240.
[25] E. Akleman, J. Chen, V. Srinivasan, F. Eryoldas, A new corner cutting scheme with tension and handle-face reconstruction (2001).
[26] D. Doo, M. Sabin, Behaviour of recursive division surfaces near extraordinary points (1978).
[27] L. Guibas, J. Stolfi, Primitives for the manipulation of general subdivisions and the computation of voronoi, ACM Trans. Graph. 4 (2) (1985) 74–123.
[28] E. W. Weisstein, Spanning Tree, From MathWorld–A Wolfram Web Resource,http://mathworld.wolfram.com/SpanningTree.html, 2013.
[29] D. Hartl, D. Lagoudas, F. Calkins, Advanced methods for the analysis, design, and optimization of SMA-based aerostructures, Smart Materials and Structures 20 (9) (2011) 094006.
[30] Abaqus, Analysis User's Manual, Dassault Systèmes of America Corp., Woodlands Hills, CA (2012).
[31] Abaqus, Theory Manual, Dassault Systèmes of America Corp., Woodlands Hills, CA (2007).
[32] T. J. R. Hughes, J. Winget, Finite rotation effects in numerical integration of rate constitutive equations arising in large-deformation analysis, International Journal for Numerical Methods in Engineering 15 (12) (1980) 1862–1867.
[33] J. Reddy, An Introduction to Nonlinear Finite Element Analysis, Oxford University Press, Oxford, UK, 2004.
[34] D. C. Lagoudas, D. J. Hartl, Y. Chemisky, L. Machado, P. Popov, Constitutive model for the numerical analysis of phase transformation in polycrystalline shape memory alloys, International Journal of Plasticity 32–33 (2012) 155–183.
[35] W. S. Slaughter, The Linearized Theory of Elasticity, Birkhäuser, Boston, 2002.
[36] G. Hart, Slide-Together Geometric Paper Constructions, Bridges, Mathematical Connections between Art and Science Conference - Workshop, 2004.
[37] J. Miller, E. Akleman, Edge-Based Intersected Polyhedral Paper Sculptures Constructed by Interlocking Slitted Planar Pieces, 11th Bridges, Mathematical Connections between Art and Science Conference. 2008. Leewardeen, Netherland,, 2008.
[38] J.-M. Lien, N. M. Amato, Approximate convex decomposition of polyhedra, in: Proceedings of the 2007 ACM symposium on Solid and physical modeling, 2007, pp. 121–131.
[39] M. Ghosh, N. M. Amato, Y. Lu, J.-M. Lien, Fast approximate convex decomposition using relative concavity, Computer-Aided Design 45 (2) (2013) 494 – 504, Solid and Physical Modeling 2012.
[40] S. Dong, P.-T. Bremer, M. Garland, V. Pascucci, J. C. Hart, Spectral surface quadrangulation, SIGGRAPH '06, 2006, pp. 1057–1066.